

Closed-Loop Control of Electrical Stimulation through Spared Motor Unit Ensembles Restores Foot Movements after Spinal Cord Injury

Vlad Cnejevici¹, Matthias Ponfick², Raul C. Sîmpetru¹, Alessandro Del Vecchio^{1,*}

¹ Neuromuscular Physiology and Neural Interfacing Laboratory, Friedrich-Alexander-Universität Erlangen-Nürnberg; Erlangen, 91052, Germany.

² Querschnittszentrum Rummelsberg, Krankenhaus Rummelsberg GmbH; Schwarzenbruck, 90592, Germany

* Corresponding author. Email: alessandro.del.vecchio@fau.de

This work was supported in part by the European Research Council (ERC) through the project GRASPAGAIN under the grant 101118089, the German Federal Ministry of Research, Technology and Space (BMFTR) through the project NOE-EMY under the grant 16SV9246 respectively, the German Research Foundation (DFG) through the project DeMOTUS and under the grant 523352235 and the Bavarian Ministry of Economic Affairs, Regional Development and Energy (StMWi) through the projects GraspAgain and NeurOne under the grants MV-2303-0006 and LSM-2303-0003.

ABSTRACT

Restoring movement of a paralyzed foot is a key challenge in helping individuals with neurological conditions such as spinal cord injury (SCI) to improve their quality of life. Neuroprostheses based on functional electrical stimulation (FES) can restore the physiological range of motion by stimulating the affected muscles using surface electrodes. We have previously shown that, despite chronic motor-complete SCI, it is possible to capture paralyzed hand movements in individuals with tetraplegia using spared and modulated motor unit (MU) activity decoded with non-invasive electromyography (EMG) sensors. This study investigated whether a wearable high-density surface EMG system could capture and control paralyzed foot kinematics in closed-loop control with an FES system. We found that all our participants with SCI (2 with chronic SCI and 3 with acute SCI) retained distinct spared EMG activity for at least three ankle movements, which allowed them to reliably control a digital cursor using their spared tibialis anterior and triceps surae MU activity. Movement separability was further reconfirmed by extracting task-modulated MU activity during foot flexion/extension (3-7 modulated MUs/participant). Three participants were further able to modulate and maintain their foot flexion/extension EMG levels with an accuracy of >70%. Lastly, we show that real-time control of a FES system using EMG from the affected limb can restore foot movements in a highly intuitive way, significantly improving the lost or pathological foot range of motion. Our system provides an intuitive approach for closed-loop control of FES that has the potential to assist individuals with SCI in regaining lost motor functions.

INTRODUCTION

Drop foot refers to the reduced ability to lift the foot due to disrupted neural pathways between the brain and lower limb muscles. This can be caused by a variety of neurological conditions, including spinal cord injury (SCI) [1], stroke [2], or peripheral nerve damage [3]. All these can consequently lead to a decrease in quality of life [3]. People with drop foot could benefit from using neuroprosthetic devices based on functional electrical stimulation (FES), which deliver electrical pulses to the affected muscles (e.g., through electrodes placed on the skin surface) [4]. The role of these systems is to assist the user during daily relevant activities and to increase the strength of their affected muscles [4].

Electrical stimulation can be triggered by an external input signal which allows the user to control the onset of the desired movement. However, the dominant approach for determining lower limb movement intent in both commercial [5], [6], [7], [8] and research-based systems [9], [10], [11], [12] still relies on foot switches, motion sensors and tilt sensors, which inherently depend on detecting the user's pathological range of motion (i.e. the remaining range of motion post-injury). Recent works [13], [14], [15], [16] have also explored controlling FES devices through surface electromyography (EMG), a non-invasive technique for measuring voluntary neural activity at the muscle-level generated by motor unit (MU) ensembles [17]. However, these works have either not validated their systems on patients [14], [15], [16] or relied on sensing the EMG activity from muscles not affected by the neural injury [13]. Therefore, the control of the FES is only indirect, relying on signals from unaffected muscles, and does not utilize the same neural commands that existed before the injury.

Alternatively, the FES system can be controlled in closed-loop using the spared and still voluntarily modulated EMG signals of the affected leg that closely reflects the user's movement intent. The movement intent is then used to stimulate the same muscles to elicit greater movement ranges. In our previous work on the upper limb, we found evidence of distinct MU ensemble activity associated with fully paralyzed hand movement using high-density EMG in both healthy individuals [18] and in people with SCI [19], [20]. Interestingly, we found that individuals with SCI, even in cases of motor-complete injuries, still retain voluntary MU activity that encodes lost hand movements. This activity was then decoded through a neural interface and used to control a virtual hand with high accuracy [19], [20]. Here, we first aimed to determine whether individuals with SCI also exhibit spared neural activity when recording EMG signals from the lower leg muscles and further assess how well this activity can be modulated. We hypothesized that if such spared neural activity is also present in the lower limb after SCI, a FES system tuned to this activity could enable a reliable and natural control of the paralyzed foot.

We recorded the spared neural activity from five individuals with motor incomplete SCI, denoted S1-S5 (S1 & 2 with chronic SCI, S3-5 with acute SCI; Table 1), using a wearable 32-channel surface EMG bracelet [20] placed below the knee (Fig. 1A). Additionally, we developed a machine-learning (ML) driven neural interface for mapping the identified motor dimension patterns to the motion of a 2D cursor on a screen. (Fig. 1B). We first demonstrated that participants could control this cursor accurately and consistently during ankle flexion and extension, as well as during inward or outward rotation of the ankle (Fig. 1C, see Motor Dimension Separation). The ability to modulate the spared neural activity during foot flexion/extension was further reconfirmed by extracting multiple MUs from the raw EMG data. These MUs showed a correlation with the requested flexion/extension movement pattern, revealing the presence of spared voluntarily

modulated MU activity in the lower limb even after SCI (see Motor Dimension Separation). Successively, we showed that S1, S2 and S5 (Table 1) could modulate and maintain their EMG activation level during flexion/extension movements, both under full and partial muscle contraction (Fig. 1D, Table 2, see Proportional Activation). Finally, two participants (S1 and S2, Table 1) used their spared voluntary neural activity to control an electrical stimulator (Fig. 1E, see Functional Electrical Stimulation) to either restore the range of motion for completely lost movements (S2, Table 1) or help them exceed their pathological range of motion (S1, Table 1). The closed-loop control of our neuroprosthetic allows paralyzed individuals to naturally control the affected foot by reading and stimulating the same muscle activity, with rapid calibration times (~30 minutes) of the stimulation control parameters (Table 3). This is possible because the source of the neural signals is the same that once controlled the paralyzed foot before the injury. By mapping the spared motor dimensions directly onto a 2D controllable digital signal, our solution provides a rapid and highly intuitive approach to assessing the level of stable EMG control retained by the individual with SCI, which in turn can inform on how best to improve the user control over the assistive system.

RESULTS

Virtual cursor-based decoding and restoration of lower limb movement

We developed a 2D cursor-based virtual interface to guide individuals with SCI in performing or attempting four foot movements: dorsiflexion/plantarflexion (i.e. foot flexing upward/extending downward) and inversion/eversion (i.e. foot sole turning inward/outward) (Fig. 2A & B). The software interface was developed in our previously published framework MyoGestic, an open-source framework for decoding spared motor dimensions from individuals with neural lesions [20].

The interface displayed a circle reference cursor that served as a visual movement guide for the participants. The cursor moved in a linear oscillating pattern along the X or Y axis (Fig. 2B), starting from the axes intersection and moving towards the axes end points and back. Movement along each axis indicated the direction that participants should follow when attempting to move their foot. This cursor interface, similar to those used in other studies on myoelectric control [21], [22], [23], was designed to allow the experimenter to easily and flexibly map foot movements to different directions for the cursor movement. Here we focused on decoding five motor dimensions for the ankle, each mapped to the cursor movement in one direction: dorsiflexion – move up, plantarflexion - move down, inversion – move right and eversion – move left and rest – stay in middle (Fig. 1B, Fig. 2B).

Table 1. Participant characteristics. Age is given in 5-year ranges to protect the participants' privacy. IL = Injury Level. ZPP = Zone of Partial Preservation [24]. AIS = ASIA Impairment Scale [24]. Dorsifl. = Dorsiflexion. Inv. = Inversion. Muscle strength was graded using the standardized scale from the Medical Research Council [25].

Subject ID	Test taken part in	Injury type (IL / ZPP / AIS)	Time since injury (y=years, m=months)	Age (5-year range)	Sex	Measured side	Dorsi-/plantarflexion muscle strength for measured (and unmeasured) sides (0-5)
S1	Motor dimension separation Proportional activation Functional electrical stimulation	Traumatic SCI L1 / S1 / D	46 y	60-64	M	right	0/3 (5/4)

S2	Motor dimension separation Proportional activation Functional electrical stimulation	Spinal cord inflammation L3 / S1 / D	4 y	60-64	M	left	0/1 (5/3)
S3	Motor dimension separation	Spinal cord inflammation L2 / S1 / D	3 m	45-49	F	left	1/3 (1/4)
S4	Motor dimension separation Proportional activation	Traumatic SCI L2 / S1 / D	1 m	55-59	F	left	1/3 (0/3)
S5	Motor dimension separation (<i>dorsifl. & inv. only</i>) Proportional activation (<i>dorsifl. only</i>)	Surgical complication L1 / S1 / C	2 m	65-69	F	left	3/2 (5/5)

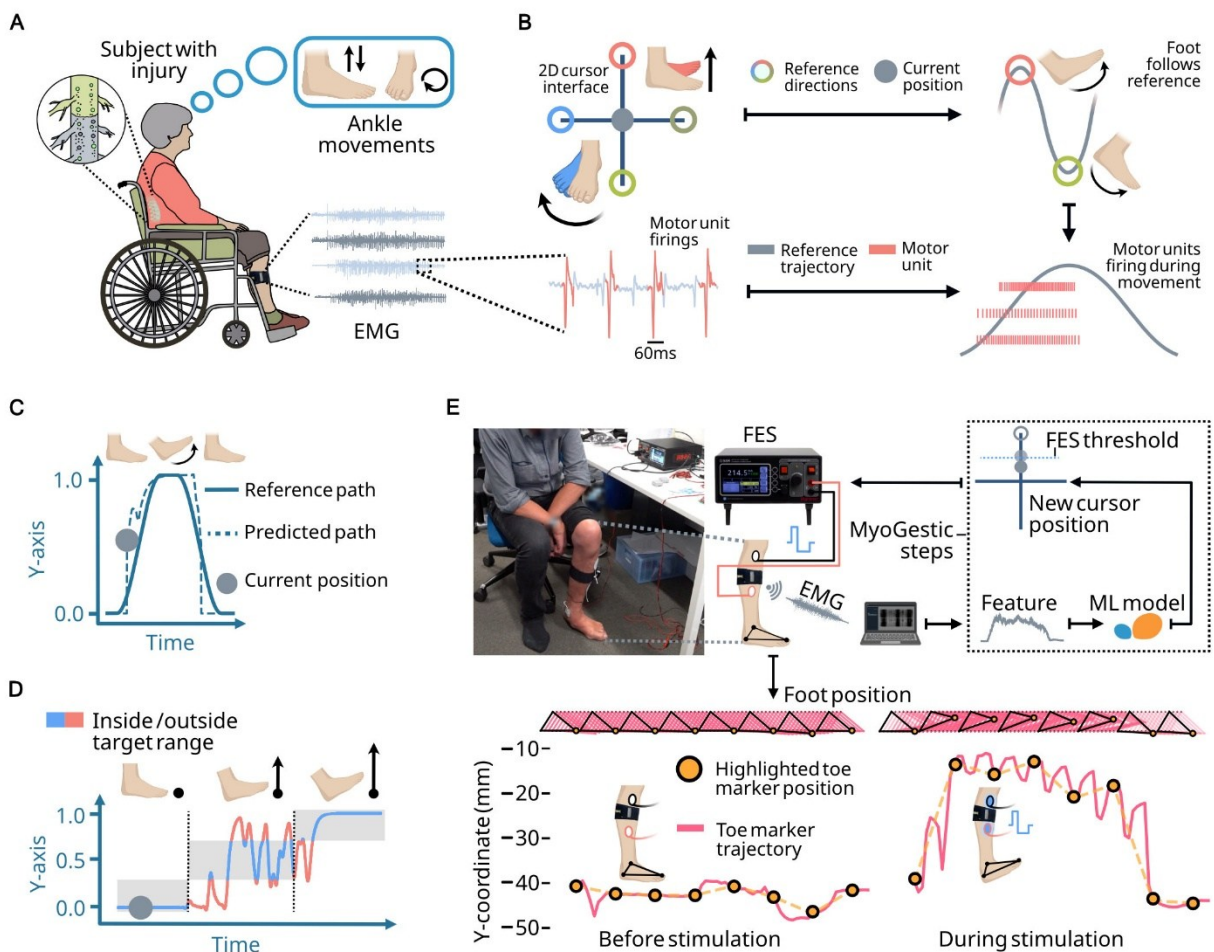


Fig. 1. Study overview. (A) Five individuals with SCI (Table 1) attempted different ankle movements while their spared MU ensemble activity below the injury level was recorded using a 32-channel surface EMG bracelet. (B) A virtual interface displaying a reference 2D cursor moving along the X- or Y-axis served as a visual movement guide. Participants followed the reference cursor during different ankle movements while their EMG was recorded and subsequently decomposed into MU firings. Example MUs with shown for S2. (C) All five participants used their spared EMG and the prediction of a model trained on that EMG to control a second cursor and follow the trajectory of a reference cursor on the screen. Example plot shown for S5. (D) Four subjects (S1, S2, S4, and S5; Table 1) attempted to partially activate their EMG by holding the predicted cursor within a margin of error covering the middle 40% of the task-relevant cursor range. Example plot shown for S4. (E) Two subjects (S1 and S2; Table 1) used their EMG activity and a Linear Discriminant Analysis model to trigger stimulation pulses from an electrical stimulator when the

predicted cursor values exceeded a threshold. The top panel shows the prediction-stimulation pipeline; the bottom shows foot movement for S1 during two contraction ramps—first ramp before (left) and first ramp during stimulation (right). Foot motion is illustrated by a 2D heel-to-toe projection and a toe trajectory plot, with matched time points marked in both.

Individuals with SCI had their spared neural activity from one of their affected lower limbs recorded using a commercially available 32-channel EMG bracelet (HD20MM1602B, OT Bioelettronica S.r.l., Turin, Italy; Fig. 1A, Fig. 2A & C; see Materials and Methods). We chose this bracelet for its wearability and its ease of use, which makes it intuitive even for individuals with limited technical experience. The EMG signals were filtered to remove noise such as motion artifacts, power line interference and high-frequency noise, after which the root mean squared (RMS) values were computed for each channel and used as features for a classification-based ML model. We used both a linear and a nonlinear model for predicting the ankle motor dimension (Fig. 2C; see Materials and Methods): a Linear Discriminant Analysis (LDA) implemented via the open-source scikit-learn ML library [26] and a Gradient Boosted Decision Tree implemented via the CatBoost algorithm as the non-linear model [27]. LDA is a well-established method for classifying EMG activity associated with different movements and has shown strong performance for ankle movement classification [28], [29], [30]. The CatBoost model was tested in our previous work [20] and was successful in predicting hand movement intent for individuals with SCI. The CatBoost model was optimized using maximum voluntary contraction data recorded from S1 during a preliminary session and from five additional healthy participants recruited for model optimization (see Materials and Methods). The optimization was performed with the Optuna software [31], achieving 300 tree iterations prior to testing the model with individuals with SCI. The results for the other optimized hyperparameters are listed in Materials and Methods.

Each ML model was trained using a single initial resting period of 10 seconds, followed by a 10-second maximum voluntary contraction recorded separately for each ankle movement. We refer to this as the offline recording. During this contraction, participants attempted to reach their full pathological range of motion and stopped at the point where the effort involved in performing the movement became too great. The preprocessed data was split into training and test sets, with the middle 20% of each recorded task being used as test data and the remaining values used as training data. A model accuracy greater than 80% on the test set indicated that we could further use the model to map the EMG to the cursor movement (see Materials and Methods). During the cursor control stage of the experiment, each new model prediction was used to calculate the position of a second cursor that was steered by the participants through their spared neural activity towards the reference cursor (see Materials and Methods).

We developed three tests involving participants in the loop (referred to as online recordings), in which they attempted to modulate their spared EMG towards different goals. Each test involved 10 seconds of a foot resting state, followed by 3-5 contraction ramps per movement adjusted based on the comfort of the participant — enough ramps to warm up if the start was difficult, but not too many as to cause fatigue.

In the first test (Fig. 1C; see Motor Dimension Separation), all five participants tracked a linear oscillating reference cursor (Fig. 2B, Fig. 3B) using a predicted cursor derived from the model prediction. An additional offline analysis of the motor dimension separation was included. This consisted of an evaluation of the model accuracy and EMG feature space separability, as well as an analysis of MU activity during dorsiflexion/plantarflexion. Meanwhile, in the second test (Fig. 1D, see Proportional Activation), subjects aimed to maintain the predicted cursor within an error margin covering the middle 40% of the task-relevant cursor range (e.g., the top half of the Y-axis for dorsiflexion). Prior to initial data collection for the experiments, participants were introduced

to the experiment setup and given time (~5 min) to practice each of the four movements while following the pace of the reference cursor displayed on the screen. This allowed us to assess for which motor dimensions could participants generate an EMG activity distinct from the resting state and helped minimize any discomfort experienced by them while performing the movements. For S3 and S5, the initial EMG recording protocol was modified to 30 seconds of slow, repeated flexion and rest (0.1 Hz), as full muscle activation was challenging for them (see Motor Dimension Separation). For S5, only dorsiflexion and inversion were tested during the online cursor control due to difficulties faced by the participant in consistently performing plantarflexion and eversion (see Motor Dimension Separation, see Proportional Activation).

In the third test, the predicted cursor position was monitored to determine whether it exceeded a threshold set by the experimenter, based on how the subject controlled the cursor, to allow for the best possible separation between movement intent and rest. If the threshold was exceeded, a train of electrical stimulation pulses was delivered to the affected muscles via electrodes placed on the surface of the skin with the goal of enhancing the range of motion (RoM) of the participant (Fig. 1E, see Functional Electrical Stimulation). The RoM achieved before and during electrical stimulation was assessed using motion tracking cameras and infrared reflective markers placed on the shin and foot (Fig. 2A & D).

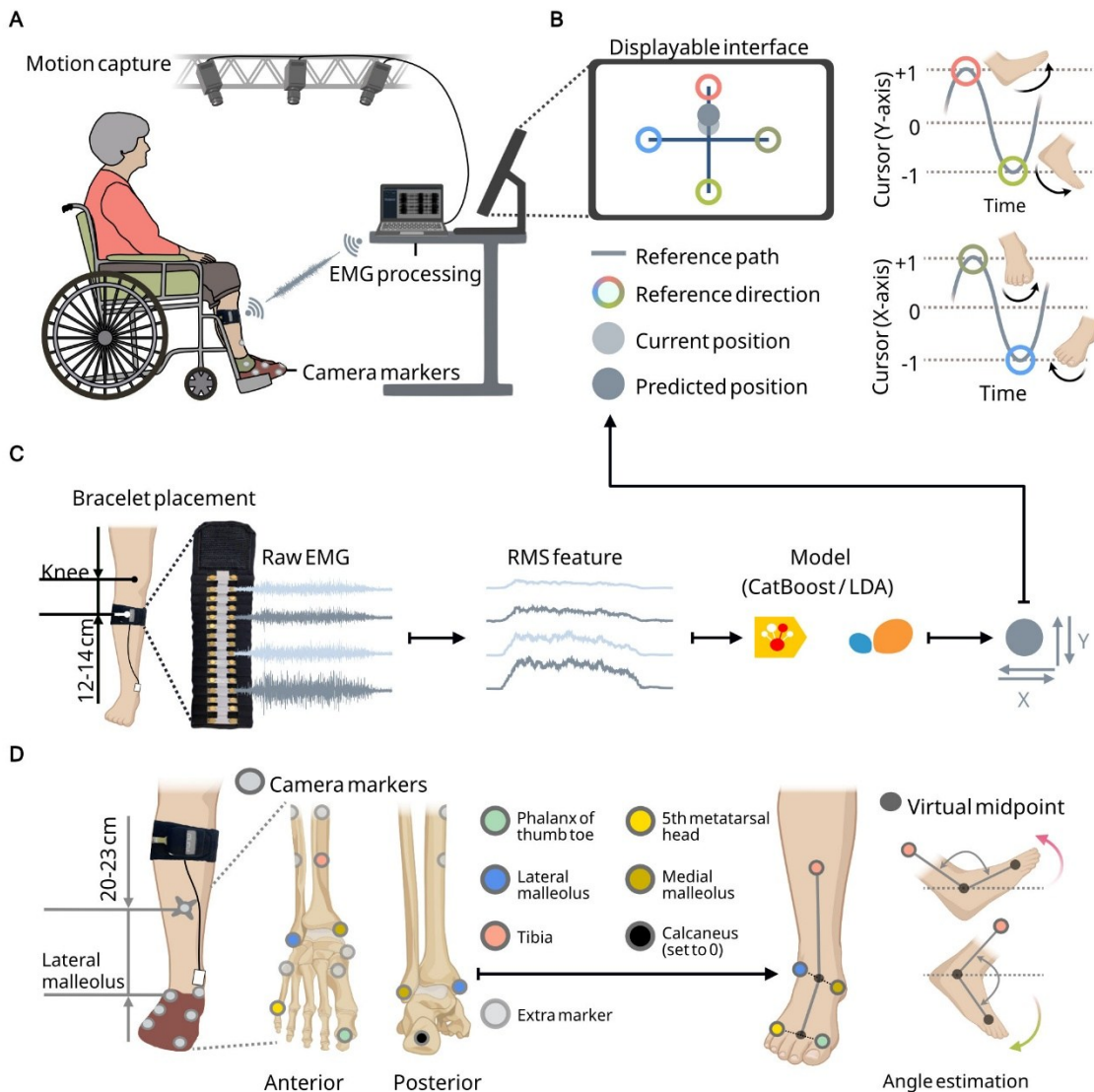


Fig. 2. Experimental setup. (A) Participants attempted ankle movements while spared neural activity was recorded using a 32-channel EMG bracelet and wirelessly streamed to a host device. For the electrical stimulation test, their ankle RoM before and while delivering stimulation pulses was captured using a motion capture camera system and infrared reflective markers placed on the shin and foot. (B) A 2D reference cursor with a linear oscillating motion in one of four X- or Y-axis directions guided participants in both pace and movement type (Y-axis for dorsi-/plantarflexion and X-axis for inversion/eversion). (C) From the recorded EMG signals, the root mean squared values (RMS) were extracted and used as features for a ML - either a Linear Discriminant Analysis or a CatBoost model (see Materials and Methods). A second EMG-controlled cursor was updated in real time based on the model predicted movement intent (see Materials and Methods). (D) Infrared markers on the shin and foot were used to compute 3D coordinates and joint angles to assess the ankle RoM. The primary camera markers (see Materials and Methods), shown in color, allowed to measure the flexion/extension angle, while the calcaneus marker corrected for the initial foot position offset. Extra markers helped reconstruct the key positions of the primary markers if occluded.

Motor Dimension Separation

Five participants with SCI (Table 1) used their spared EMG to control the position of a cursor and followed the trajectory of second reference cursor (Fig. 1C, Fig. 3B, Movie S1) while attempting four different ankle movements (Fig. 2B, Fig. 3A): dorsi-/plantarflexion (foot flexing upward/extending downward) and inversion/eversion (foot sole turning inward/outward). The intersection of the X and Y axes was mapped to the foot resting state, while the axis endpoints were each mapped to a full muscle activation of one ankle movements (Fig. 3A). Our aim was to determine if the motor dimensions for dorsi-/plantarflexion could be distinguished from other

ankle movements. This would help minimize false positives in motor intent prediction when controlling the FES system via EMG. We hypothesized that a good separation of spared ankle motor dimensions would translate into a stable low-error control of the cursor.

During the collection of model training data, participants were instructed to attempt a maximum voluntary contraction for 10 seconds during each ankle movement. For S3, however, maintaining the contraction proved too difficult and the protocol was therefore adapted to 30 seconds of repeated contraction and rest. The reference cursor, serving as a movement guide, was oscillating linearly (Fig. 2B, Fig.3B) on the screen at 0.1 Hz and stopping for every oscillation cycle at the rest and full contraction position for 0.5 seconds each. The same adjustment was made for S5, who found it difficult to consistently generate EMG activity beyond rest levels during plantarflexion and eversion. Since the offline accuracy for S5 was also lower (<80%) than that of other participants, the protocol was further adapted to include only rest, dorsiflexion and inversion for the cursor control with 2 second ramps for both contraction and rest to minimize the participant's fatigue.

Model accuracy was assessed using both test data from the initial EMG recordings (offline analysis, Fig. 3C) and data recorded during the cursor control phase (online analysis, Fig. 3D). For the offline analysis (Fig. 3C), the first two LDA components are shown, which were aligned across the subjects using Procrustes analysis [32]. In addition, the normalized mean absolute error (nMAE) metric was used for the online analysis to assess how close subjects were able to steer the EMG-controlled cursor to the reference cursor. This was calculated by first normalizing the cursor coordinates between -1 and +1 on the X and Y axis respectively (Fig. 3A). The task was defined to start when the reference cursor crossed ± 0.5 on either axis, while the initial movement of the cursor served as a visual cue for the subject to prepare for the task. As we aimed to assess only one motor dimension at a time, we restricted the predicted cursor position to one axis based on the most active motor dimension (Fig. 3A).

Healthy participants (see Materials and Methods) only took part in this test and their online results indicated a small enough error to justify testing the models further (nMAE = 0.15 ± 0.11 for LDA and 0.18 ± 0.13 for CatBoost). The nMAE values obtained by each subject with SCI are as follows: 0.24 ± 0.39 for S1, 0.25 ± 0.41 for S2, 0.23 ± 0.32 for S3, 0.17 ± 0.3 for S4 (Fig. 3B) and 0.09 ± 0.19 for S5 (dorsiflexion, inversion & rest only). Meanwhile, the task nMAE values across all subjects with SCI and models (Fig. 3E) are as follows: 0.15 ± 0.10 for rest, 0.08 ± 0.05 for dorsiflexion, 0.17 ± 0.13 for plantarflexion, 0.37 ± 0.31 for inversion and 0.26 ± 0.26 for eversion. Finally, the mean error achieved while using the LDA and CatBoost was 0.19 ± 0.2 and 0.22 ± 0.22 respectively.

To further assess motor dimension separability, we recorded 30 seconds of data from all subjects for both dorsiflexion and plantarflexion, while they were performing contraction ramps following the 2D reference cursor. The cursor moved at 0.1 Hz, while for each contraction ramp the cursor position was maintained for 0.5 seconds during full contraction and 0.5 seconds during the resting state. The recorded EMG signals were decomposed using the convolution kernel compensation method (see Materials and Methods) into MU firings. The discharge rate of the MU firings was smoothed with a Hann window of 500ms as proposed in Negro et al. [33] and correlated with the reference signal. We identified the presence of unique, task-modulated MUs associated with specific ankle motor dimensions—such as MUs that were active only during specific attempted movements (Fig. 4). By decomposing the EMG signals from all participants, we quantified the number of modulated MUs related to foot flexion and extension as follows: 7 MUs for participant S1 (1 for flexion, 6 for extension), 6 MUs for S2 (3 for flexion, 3 for extension), 3 MUs for S3 (1 for flexion, 2 for extension), 5 MUs for S4 (3 for flexion, 2 for extension), and 4 MUs for S5 (all

for flexion). The results for participants S1, S2, and S4 are presented in Fig. 4, while those for S3 and S5 are shown in Fig. 5.

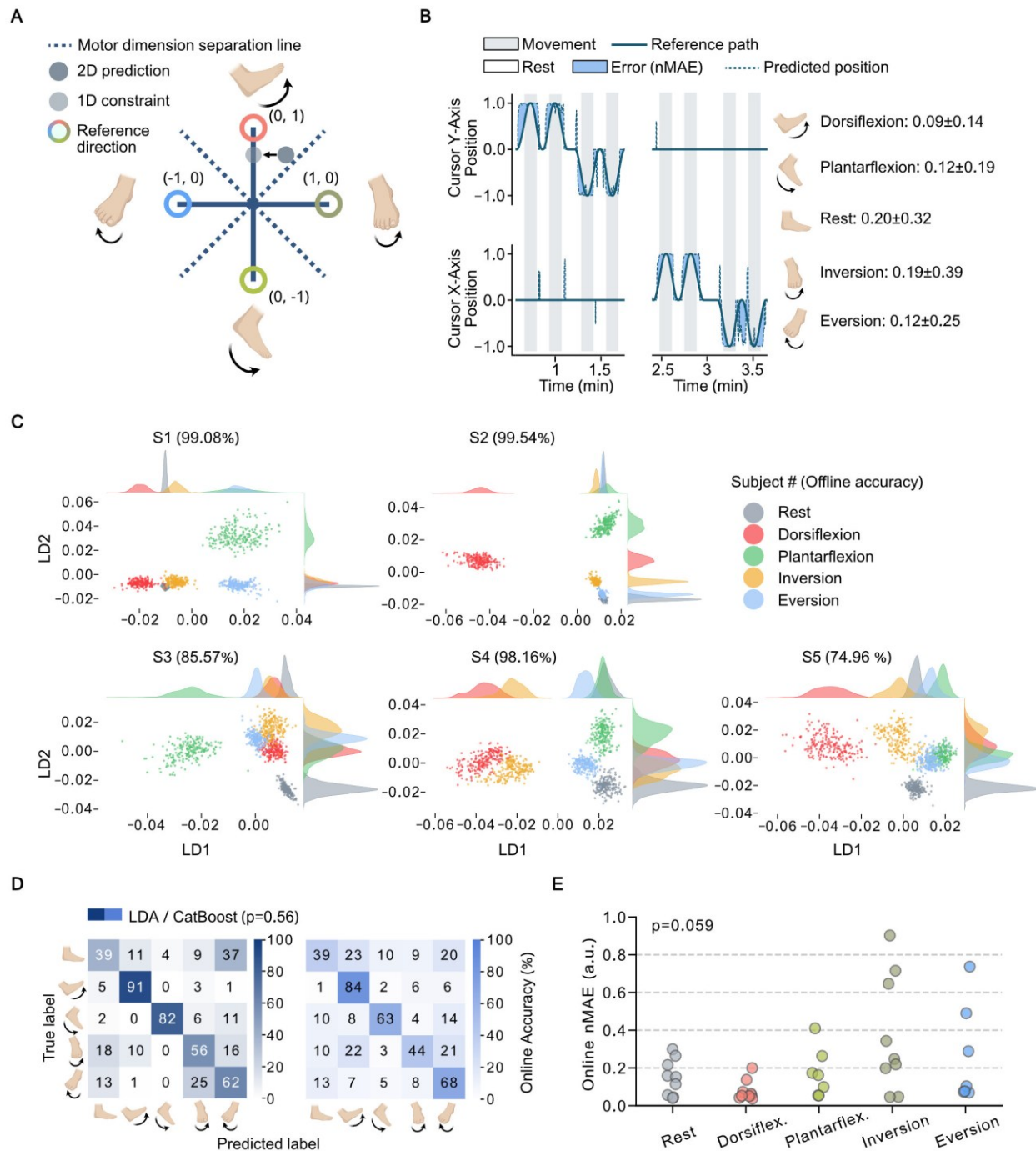
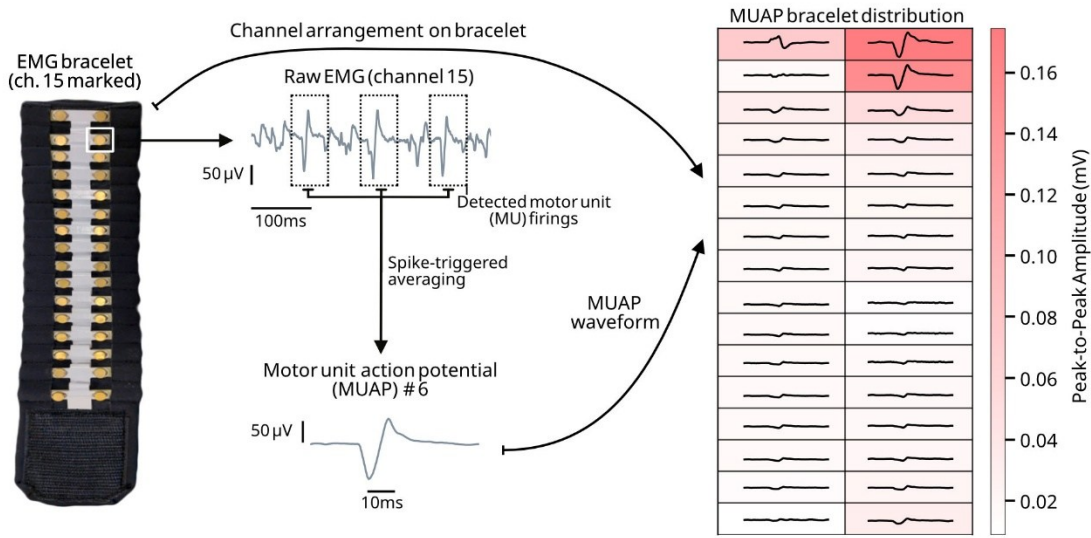


Fig. 3. Overview of motor dimension separation test. (A) All participants attempted different ankle movements while following a reference cursor (coordinates normalized between -1 and +1) along the X-axis (for inversion/eversion) or Y-axis (for dorsiflexion/plantarflexion). Based on the ML model prediction, the position of a second cursor was updated incrementally (see Materials and Methods). During post-processing, X-Y quadrants were defined to constrain the predictions to the dominant identified motor dimension. (B) The normalized mean absolute error (nMAE), computed as the L1 distance between the prediction and reference cursor positions, was used to assess how well participants followed the reference cursor. Example predictions and reference cursor trajectories are shown for S4. (C) The first two LDA components derived from the EMG test data recorded offline for each subject, along with the kernel density estimates and offline results, are shown at the top for each subject. (D) Online accuracy results for

all participants using the LDA (left) and CatBoost (right) models. Statistical test analysis by Mann-Whitney U test ($\alpha=0.05$). (E) Online task performance across all models and subjects. Statistical test analysis by Kruskal-Wallis test ($\alpha=0.05$).

A



B

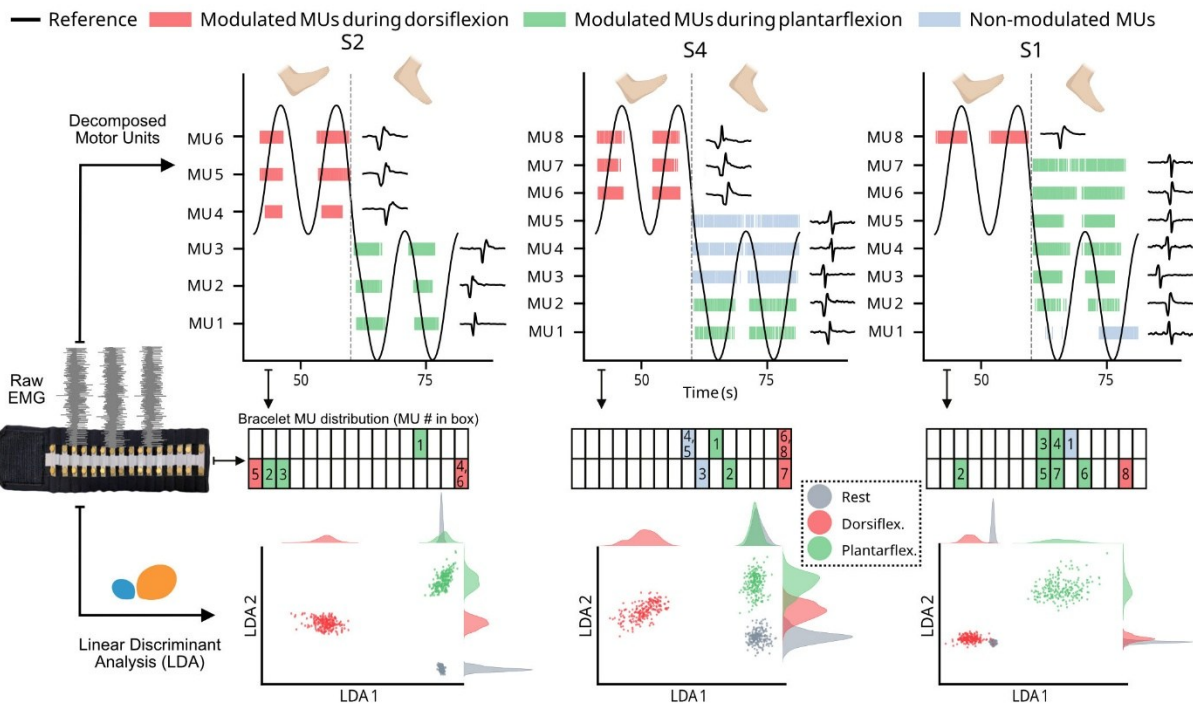


Fig. 4. Example of MU activity during foot dorsi-/plantarflexion. (A) Raw EMG data was recorded during foot dorsi-/plantarflexion (here shown for S2, Table 1) and decomposed to identify spared MU activity. Signals from channel 15 of the 32-channel bracelet (left) are shown over a 0.4-second window (middle-top), with dashed boxes marking firings of MU 6. The corresponding action potential waveform, derived via spike-triggered averaging over a 60 millisecond window (middle-bottom), is shown propagating across bracelet channels over a heatmap of MU action potential peak-to-peak values (right). (B) Task separability for three subjects (S2, S4, S1, Table 1) is illustrated using the following: decomposed MU pulse trains with corresponding MU action potentials (top), spatial distribution of MUs across the bracelet channels according to location of largest peak-to-peak values (middle) and a 2D LDA projection of the EMG feature space for the model training data (bottom). All identified MUs are shown during two contraction ramps. The smoothed discharge rate of each MU was correlated with the reference Y-axis cursor movement. A Pearson correlation coefficient >0.5 indicated MU task modulation, while <0.5 indicated non-modulated MUs.

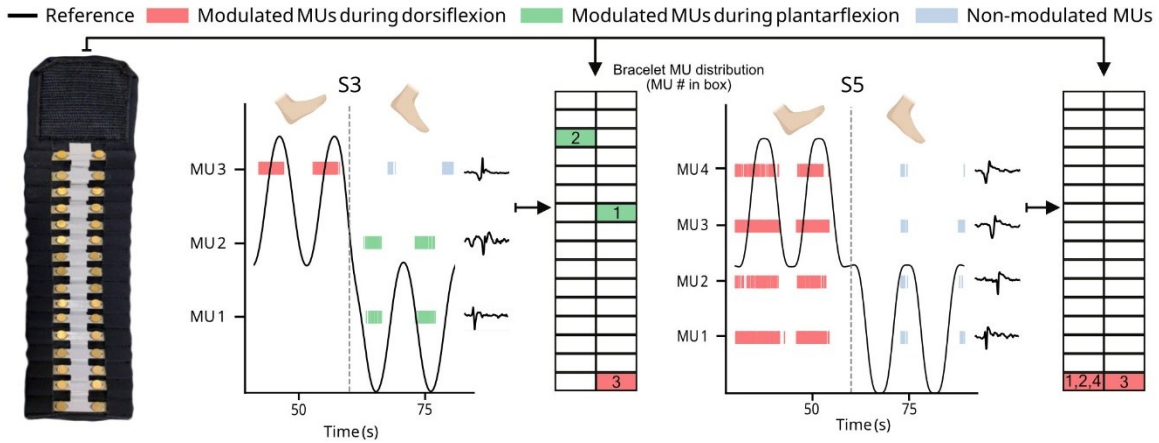


Fig. 5. Decomposed motor unit data from subjects S3 and S5, including the motor unit pulse firing during foot flexion/extension and the bracelet spatial distribution of the most significant channels for each motor unit based on the peak-to-peak amplitude.

Proportional Activation

Four participants with SCI (S1, S2, S4 and S5; Table 1) attempted to maintain a partial dorsi-/plantarflexion by holding the predicted cursor within a rectangular frame displayed in the visual interface (Fig. 1D, Fig. 6A, Movie S2). The aim was to determine if participants retained the ability to proportionally flex and extend their foot by reaching and holding two stable levels of EMG activation. This would further inform us if proportional control would be sufficiently stable for FES control. For S5, only dorsiflexion was tested due to difficulty faced by the participant in generating an EMG pattern for plantarflexion distinct from the resting state (see Motor Dimension Separation).

The ML models were only trained on rest and on dorsi-/plantarflexion data. As the cursor transition was smoothed from one position to another based on the ML model prediction (see Materials and Methods), partial EMG activation would result in a fluctuation between the positions mapped to rest and full contraction. We hypothesized that a smaller fluctuation of the EMG-controlled cursor around a given target (represented by the reference cursor at the midpoint between rest and full contraction) indicated a more stable partial EMG activation. The rectangular frame, covering the middle 40% of the task-relevant cursor range (e.g., the top half of the Y-axis for dorsiflexion), represented a margin of error within which participants attempted maintaining the predicted cursor through their EMG (Fig. 6A). Participants followed the reference cursor along 2-stage trapezoidal ramps that progressed through rest, midpoint, full contraction, midpoint, and back to rest. The cursor would remain in each of these states for 10 seconds. For performance assessment, the Y-semiaxes ranges for dorsiflexion and plantarflexion were each divided into 3 ranges: 0 to $\pm 30\%$ for rest, ± 30 to $\pm 70\%$ for partial activation and ± 70 to $\pm 100\%$ for full activation (Fig. 6A).

For each predicted cursor position, a label was assigned to the position indicating “Correct” if the position was within the task designated area or “Incorrect” if outside of it (Fig. 1D, Fig. 6A). Accuracy for each task was calculated as the number of “Correct” labels over the total number of labels. Furthermore, to assess whether the ability to stay within the rectangular frame reflected a proportional modulation of EMG activity, we computed the Jensen-Shannon divergence [34] over the probability distributions of the EMG RMS values (Fig. 6A). This metric assesses the inherent

distinctiveness between the distribution of EMG activation levels independent of the model performance. The accuracy and divergence are shown in Fig. 6B & D, along with the Pearson correlation coefficient and statistical significance level in Fig. 6D.

The accuracy for each subject is shown in Table 2, while the results for the best performing models for each subject are shown in Fig. 6B and Fig. 6C (along with time passed since the injury occurred). The overall task accuracy across all subjects and models (Fig. 6E) is the following: 75.70% \pm 23.46% for dorsiflexion, 49.18% \pm 24.49% for partial dorsiflexion, 69.92% \pm 22.05% for plantarflexion and 35.13% \pm 17.21% for partial plantarflexion.

Table 2. **Task accuracy for each subject and ML model.** The results for the best performing model for each subject are highlighted.

Subject ID	Overall accuracy (%)	Dorsiflexion accuracy (%)		Plantarflexion accuracy (%)		Rest accuracy (%)
	LDA (CatBoost)	Full activation	Partial activation	Full activation	Partial activation	
S1	78.45 (44.61)	93.13 (96.50)	69.64 (54.81)	93.69 (95.25)	57.38 (21.78)	94.14 (26.70)
S2	37.33 (70.13)	19.73 (70.64)	11.10 (38.89)	62.36 (71.80)	40.14 (56.42)	47.65 (98.67)
S4	53.59 (46.12)	67.58 (94.32)	36.86 (22.11)	67.06 (29.39)	15.67 (19.40)	77.55 (70.36)
S5	84.61 (84.82)	78.73 (84.93)	82.06 (77.96)	N/A	N/A	92.92 (91.97)

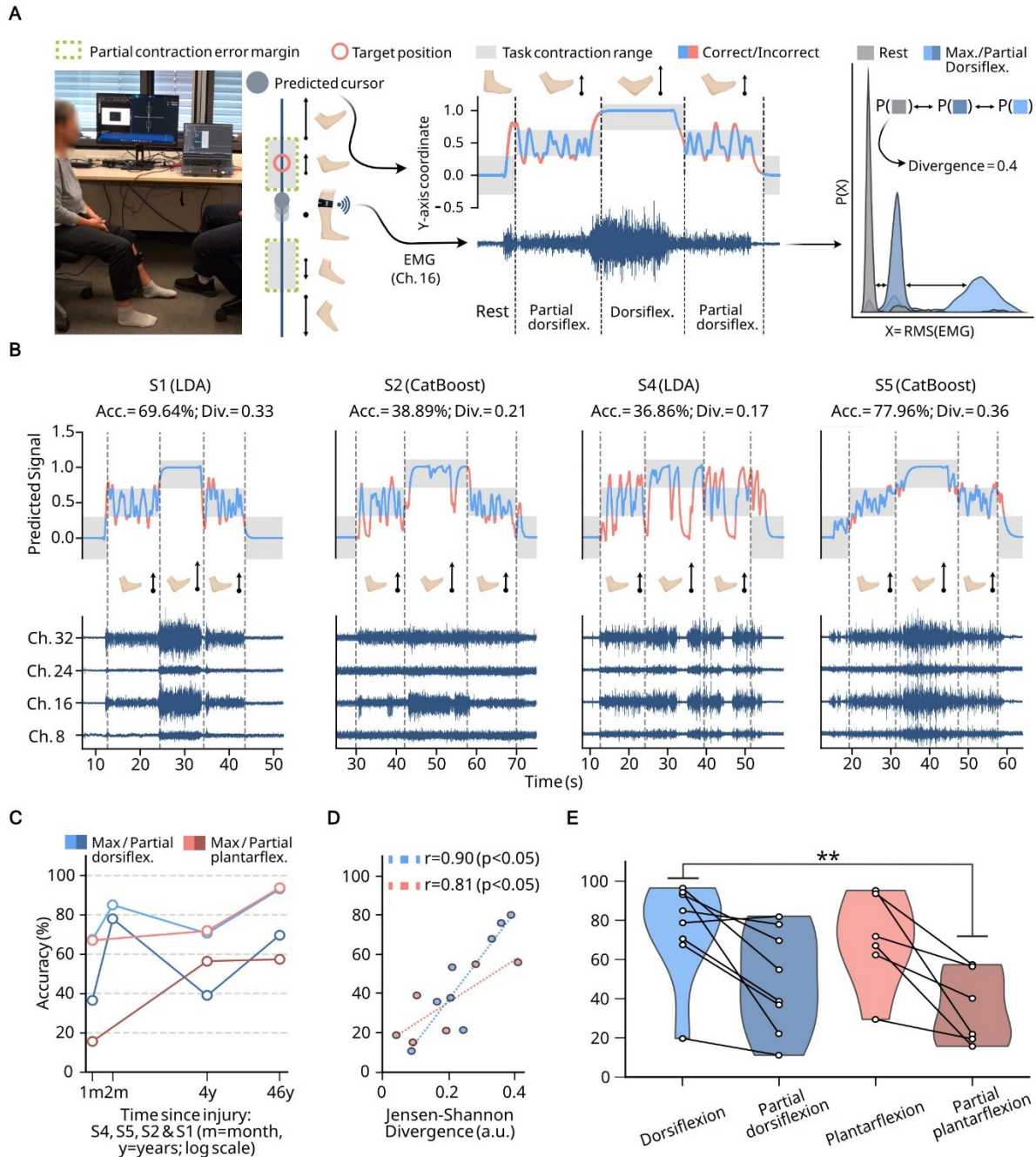


Fig. 6. Overview of proportional activation test. (A) Four participants (S1, S2, S4, S5, Table 1) aimed to hold the predicted cursor within a $\pm 20\%$ error margin on the task-relevant axis range. Accuracy, as shown for S1 using the LDA, was computed using the predicted cursor positions inside and outside of the cursor target ranges, while the Jensen-Shannon divergence assessed distribution distinctiveness of the EMG root mean squared (RMS) values (here shown for channel 16). (B) Predicted signal example during full and partial dorsiflexion for each subject using the best performing model (top). Below are shown the task accuracy and Jensen-Shannon divergence for partial dorsiflexion (top), the predicted Y-axis trajectory with target ranges (middle) and four EMG channels (bottom). (C) Task accuracy shown for each subject and their best performing model (LDA for S1 and S4, CatBoost for S2 and S5, Table 2) plotted against time since the injury (logarithmic scale and in chronological order: S4, S5, S2 and S1). (D) Correlation between accuracy and Jensen-Shannon divergence achieved for partial dorsi-/plantarflexion for each subject and model. Statistical test analysis by Pearson correlation coefficient ($\alpha=0.05$). (E) Task accuracy across all subjects and models. The white dots represent the accuracy for each subject and model. Statistical test analysis by Kruskal-Wallis test ($\alpha=0.05$) followed by post-hoc two-sided Mann-Whitney U tests ($\alpha=0.05$) with Bonferroni correction. ****** $P<0.01$.

Functional Electrical Stimulation

Two participants with SCI (S1 and S2; Table 1) used EMG signals from their affected leg muscles to voluntarily control an electrical stimulator in closed-loop. They continuously triggered and stopped trains of stimulation pulses during dorsiflexion and plantarflexion using their EMG activity as represented by the 2D predicted cursor (Fig. 1E, Fig. 7B, Movie S3). The goal was for participants to voluntarily initiate stimulation using spared EMG activity to increase their RoM beyond their pathological limit.

Participants had their EMG and motion activity recorded once before applying electrical stimulation and once during the use of stimulation. The duration of the rest and contraction phases was set to 10 seconds each, while the movements were performed bilaterally to evaluate how the RoM of the more affected foot changed during stimulation compared to the less affected foot. To assess which of the participant's legs would be considered more or less affected, we used the muscle strength grading system (from 0 to 5) provided by the Medical Research Council [25]. For S1 and S2, the EMG measured side (muscle grade = 3 for S1 during plantarflexion and ≤ 1 otherwise, Table 1) was significantly more affected than the non-measured side (muscle grade ≥ 3 , Table 1). A muscle grade of 1 indicates the ability to activate the muscle but without achieving full range of motion during dorsi-/plantarflexion, while a muscle grade of 3 indicates the ability to achieve full range of motion against gravity.

The LDA model was used for this test, while the length of the recorded training data was extended to 20 seconds for each task to ensure the model prediction was stable. Before stimulation, the achieved nMAE for controlling the cursor during dorsiflexion and plantarflexion was 0.04 ± 0.11 and 0.04 ± 0.09 for S1, while for S2 it was 0.17 ± 0.32 and 0.06 ± 0.16 . This indicated a stable enough model performance to further use for controlling the stimulator.

Infrared camera markers (PrimeX 22, OptiTrack, NaturalPoint, Inc., Corvallis, Oregon, USA) were placed on both legs of the participant at key locations on the foot and tibia (Fig. 2D, Fig. 7A, see Materials and Methods) to estimate the joint RoM during dorsiflexion and plantarflexion. Markers were also placed on the unmeasured side to provide joint angle baselines for comparison with the observed changes on the measured side.

Participants S1 and S2, both with prior FES-orthosis experience (for S1, an L300 Go, Bioness Medical, Inc., Valencia, California, USA), underwent a calibration procedure where the stimulation current gradually increased from 0 mA to determine the maximum current required to elicit a visible dorsi-/plantarflexion without causing them any pain or discomfort (Table 3, see Materials and Methods). For S2 there was no visible movement elicited during plantarflexion other than a reported feeling of tension in the stimulated muscles and, as such, this movement was not further evaluated with stimulation.

The electrical stimulator we used was the DS8R (Digitimer Ltd, Welwyn Garden City, United Kingdom), an constant-current stimulator suitable for benchtop use (~ 2.1 kg, see Materials and Methods). We chose the device as it allows fine control over pulse parameters and step sizes (e.g., 0.1mA current step size) and the stimulation can be directly triggered from an external device. Here we used the Raspberry Pi 4B development board (Raspberry Pi Foundation, Cambridge, United Kingdom) to trigger the stimulator, while the control interface—linking the model prediction to the stimulator—was configured through a newly developed tab in MyoGestic (Fig. 7B). This tab allowed for instant adjustment of four parameters for fine-tuning the user control of the stimulation (Table 3):

- The trigger threshold which indicated a value on the cursor Y-axis between 0% (mapped to the resting state) and 100% (mapped to the maximum contraction) to clearly separate the intent to move the foot from the resting state and from involuntary muscle activations, as caused by spasticity [35],
- The stimulation pulse frequency, adjusted to balance between a sustained muscle contraction and maintaining a stable transmission rate between the MyoGestic software on the host device and the external development board,
- The stimulation and waiting time allowed the configuration of the stimulation pulse train duration and the after-pulse train pause, which were set to ensure the subject reached the full range of motion while keeping the system responsive to their movement intent. Alternating between stimulating and not stimulating also ensures the participant is not exposed continuously to stimulation, thus reducing the likelihood of muscle fatigue.

During the test, each predicted cursor position and the current stimulation parameters were continuously streamed from the virtual interface to the external device. When the cursor position exceeded the trigger threshold, a stimulation pulse train was delivered, followed by a pause with no stimulation. The stimulation and waiting time parameters were used to define the duration of these two phases. Cursor updates were paused during both phases and resumed afterward to assess whether the user intended to move or rest. A visualization of this process can be seen in Fig. 7B.

Joint angle values of the ankle for the measured and unmeasured sides are shown in Fig. 7C. To estimate the impact of RoM change, we took the typical RoM for dorsi-/plantarflexion (tRoM) as reported in literature [36] for older populations above the age of 60 years (similar to the ages of S1 and S2, Table 1). The chosen tRoM for normal gait was 20 degrees for dorsiflexion and -8 degrees for plantarflexion [36]. The RoM for dorsiflexion increased from 2.79 ± 1.93 to 9.51 ± 1.18 degrees (33.6% of tRoM increase) for S1 and from -0.31 ± 0.52 to 7.69 ± 2.68 degrees (40% of tRoM increase) for S2, while for plantarflexion for S1 it increased by -7.84 ± 1.79 to -8.90 ± 1.17 degrees (13.25% of tRoM increase). The resting RoM for both participants remained within 1 degree from the initial foot position. Meanwhile, the RoM for the resting state changed when applying stimulation from 0.19 ± 1.88 to 0.76 ± 0.48 degrees for S1 and from -0.06 ± 0.84 to -0.12 ± 0.50 degrees for S2, while during plantarflexion it changed from -0.05 ± 0.14 to 0.06 ± 0.08 degrees.

In addition, the Pearson correlation coefficient between the measured and unmeasured foot before and while applying stimulation are shown in Fig. 7D. The correlation between the dorsi-/plantarflexion angle of the measured and unmeasured feet across all contraction ramps increased with the use of FES compared to without FES ($p < 0.001$) as follows: for dorsiflexion, from 0.3 to 0.87 for S1 and from -0.15 to 0.6 for S2 respectively, while during plantarflexion from 0.9 to 0.96 for S1.

Table 3. Stimulation parameters for each subject. Values are displayed for dorsiflexion (& plantarflexion).

Subject ID	Stim. Current (mA)	Cursor trigger threshold (%)	Stimulation time (s)	Stimulation waiting time (s)	Stimulation frequency (Hz)
S1	53 (42)	50 (50)	1.2 (1.2)	0.4 (0.5)	25 (25)
S2	90 (N/A)	50 (N/A)	1.2 (N/A)	0.7 (N/A)	15 (15)

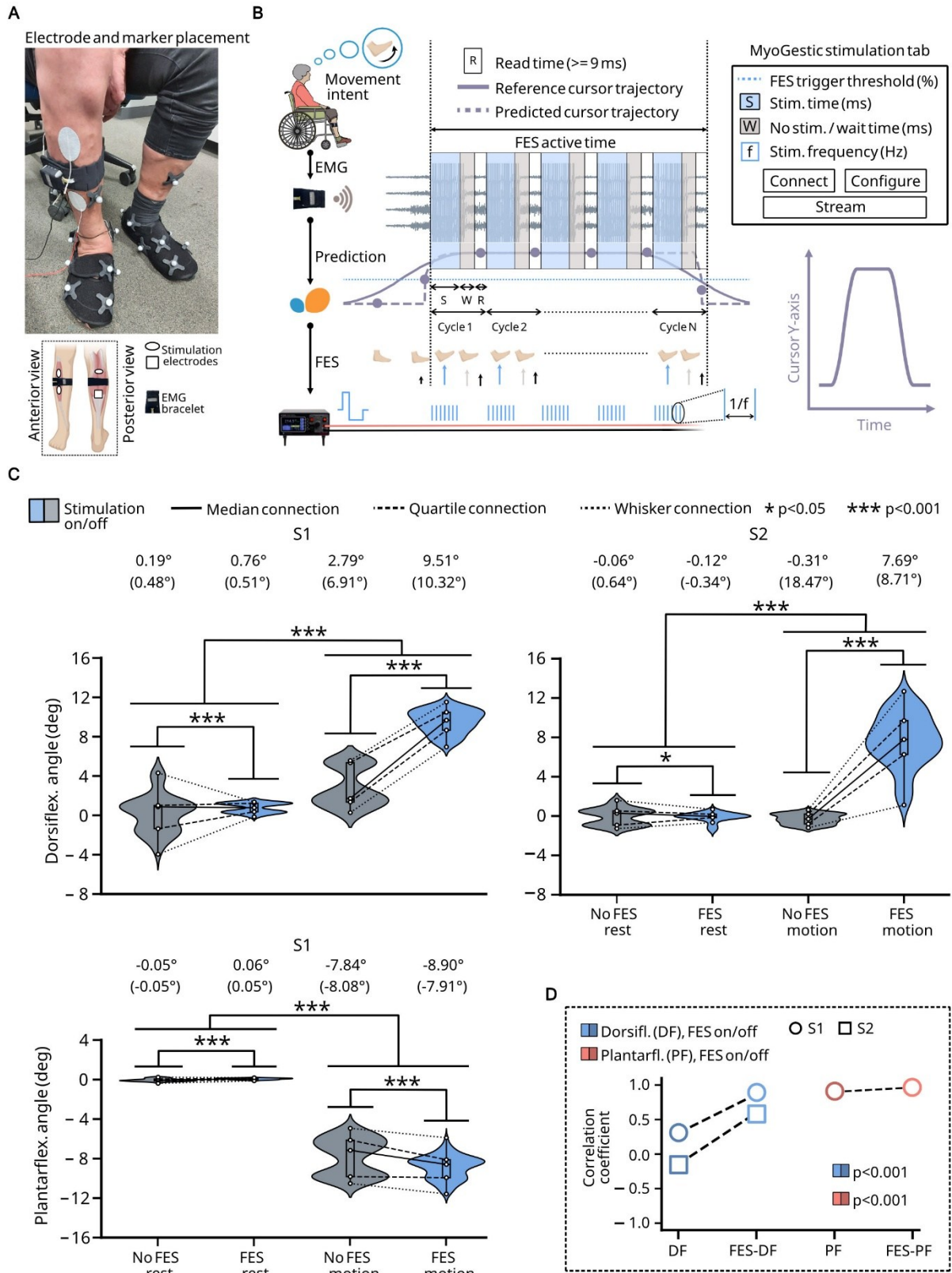


Fig. 7. Overview of functional electrical stimulation test. (A) The EMG bracelet was placed below the knee over the muscle bellies of the measured leg, while stimulation electrodes were positioned above and below the bracelet on the anterior and posterior sides of the same leg. Infrared camera markers were placed on both legs (Fig. 2D) to capture the participant's ankle RoM before and during stimulation. (B) Electrical stimulation was triggered when the predicted cursor position derived from the LDA model

prediction exceeded a subject-specific Y-axis threshold set by the experimenter. Three additional stimulation control parameters were configured for each participant: stimulation time (i.e. stimulation duration once the cursor exceeded the threshold), wait time (i.e. stimulation pause following the stimulation time) and stimulation pulse frequency. The predicted cursor position was read again following the wait time to determine if the stimulation cycle should be repeated. **(C)** Ankle joint RoM before and during stimulation for S1 and S2 during dorsi-/plantarflexion (S2: dorsiflexion only). The average RoM during the contraction ramps and rest phases is shown at the top of each plot for the measured (and unmeasured) side. Statistical analysis by one-way ANOVA ($\alpha=0.05$), followed by post-hoc independent Welch t-tests with Bonferroni correction. * $P<0.05$, *** $P<0.001$. **(D)** Correlation coefficient between the motion of both legs before and during stimulation for dorsi-/plantarflexion (S2: dorsiflexion only). Statistical analysis by Pearson correlation coefficient ($\alpha=0.001$).

DISCUSSION

Our study demonstrates the potential of our 2D cursor-based neural interface to decode the spared neural activity of the lower limb in individuals with SCI (S1-S5, Table 1) and assist them in modulating their ankle lower limb activity. In addition, we demonstrated for two of these individuals (S1 and S2, Table 1) the ability for closed-loop stimulation of the foot with direct EMG activity from the affected limbs. This system restored the ankle movements in these individuals and/or significantly increased their ankle RoM beyond their pathological RoM ($p < 0.001$, Fig. 7C).

Motor Dimension Separation

We showed that all participants exhibited distinctive patterns for three out of the five tested motor dimensions (dorsi-/plantarflexion, inversion/eversion, rest, Fig. 3C). In addition, participants successfully controlled a 2D cursor in real time with their spared EMG while following a separate reference cursor and could separate the motor dimension for dorsiflexion from the other tested motor dimensions (Fig. 3C&D). The mean error achieved across all tested movements was below 0.4 (Fig. 3E). These results suggest that even in cases where foot drop occurs after spinal cord injury, the intent to lift the foot can still be separated from other ankle movement intents and from the intent to rest, making EMG a viable option for drop foot correction systems.

Participants achieved a comparable accuracy when using the LDA or the CatBoost models (Fig. 3D), as well as a comparable task error when controlling the 2D cursor. This reconfirms the findings from other works that lower limb movement intent can be predicted from the voluntary EMG signals using an LDA [28], [29], [30] or a gradient boosted tree model [37], [38]. However, our work is, to the best of our knowledge, the first to validate and compare the performance of the LDA and CatBoost algorithms in predicting ankle movement intent in human individuals with SCI.

In the decomposed MU data for subjects S2, S4, and S1 (Fig. 4), distinct motor units are recruited and de-recruited during dorsiflexion and plantarflexion. Their firing patterns correlate with the intended cursor movements, as indicated by the reference signal in Fig. 4B. This supports our previous findings for hand movements in Souza de Oliveira et al. [39] and Osswald et al. [40] that flexion-extension movements are encoded by distinct task-modulated MUs in both healthy individuals and in those with SCI. As shown in Fig. 5 for S3 and S5, some MUs identified during dorsiflexion also fire during plantarflexion; however, these firings occur closer to the extension resting phase than to the full contraction phase. This may suggest that dorsiflexion-related motor units remain active for these participants also when they attempt to return to the foot resting state from full plantarflexion, perhaps as a way to overcome a stiff plantarflexed foot in the advent of spasticity.

We observed that S5, for whom the cursor control test was adapted, achieved the most stable control of the cursor during dorsiflexion and inversion of the foot using either ML model. The results in Fig. 3C from the offline analysis further show that overlap between motor dimensions occurred only between plantarflexion and eversion, which were also the movements that were removed in the online phase due to the cursor control of the participant being unstable during these tasks. This could indicate that an offline analysis of the training data may be suitable to identify spared neural signals for different motor dimensions. The model can then be retrained on those motor dimensions unique to each participant and enhance the system control of the user in an online setting.

Our results also show that inversion and eversion were both harder to control and more likely to be misclassified for other ankle motor dimensions (Fig. 3C, Fig. 3E). This can, in part, be explained by the biomechanical role that inversion/eversion serves during gait. Dorsiflexion and plantarflexion allow the leg to swing freely and to push off the ground when lifting the toes. Meanwhile, inversion and eversion serve a supporting role during gait by correcting individual walking variations, regulating ankle muscle effort and shifting the center of mass of the body during walking [41], [42]. Poor distinction between dorsiflexion and inversion can also be due to the tibialis anterior muscle being active during both movements, while other inversion-specific muscles such as the tibialis posterior are located much deeper in the leg and thus more likely to be recorded as crosstalk in the EMG signal [17].

Proportional Activation

We show that four participants with SCI (S1, S2, S4 and S5, Table 1) were able to achieve a moderate ($> 50\%$ for S4, Table 2), good ($> 70\%$ for S2, Table 2) and very good ($> 80\%$ for S1 and S5, Table 2) control of their EMG activation during full dorsi-/plantarflexion. Participants S1, S2 and S5 were also able to maintain this activation for over 10 seconds, regardless of the time elapsed since their injury (Table 2), as can be seen in Fig. 6B and Fig. 6C. This shows that, even shortly after the injury (2 months post injury for S5, Table 1, Movie S2), individuals with SCI may exhibit a stable enough control of some of their motor dimensions when fully activated to potentially control an external system.

For partial EMG activation, the results indicate a wide variability in the achieved accuracy (Table 2), ranging from difficulty in controlling the cursor ($< 50\%$ for S4, Table 2) to moderate control ($> 50\%$ for S1 and S2, Table 2) and to very good control ($> 80\%$ for S5, Table 2). We further evaluated how well the ability to maintain the cursor position within the rectangular frame on the screen reflected proportional control. This was done by correlating the test accuracy achieved during the experiment and the Jensen-Shannon divergence of the EMG partial activation to the full and rest activation. The results in Fig. 6B&D show a strong correlation between the two metrics ($r > 0.8$ for dorsi- and for plantarflexion, $p < 0.05$), which could suggest that the achieved performance in controlling the cursor was strongly dependent on the ability of the participants to consistently modulate their EMG after the injury.

The visualization of the predicted cursor signal and the EMG in Fig. 6B highlights how strongly this partial EMG activation differs from subject to subject. For example, the EMG of S1 (46 years post-injury) shows two separate levels of muscle activation distinct from the resting state, while for S4 (1 month post-injury) it appears that muscle activation is switching more often between the full and rest activation in an on/off manner. Since motor recovery in SCI, either natural or exercise induced, occurs the most within the first 6 months after the injury [43], [44], it is possible that individuals with SCI prior to that point may require more time and rehabilitation in order to be

able to proportionally control their muscle activity. An exception to this hypothesis is S5, who by the time of recording had already exhibited a rapid recovery in muscle strength (muscle grade of 3 two months post-injury, Table 1) and achieved very stable control of the cursor (Fig. 6B&C). Meanwhile, all other participants in this test have shown an improvement in EMG proportional control if more time has passed for them since their injury (Fig. 6C). Our findings here and in our previous work [45] highlight the benefit of using EMG as a technique for assessing proportional motor control after SCI and could have significant implications for the integration of EMG measurements into assistive devices that aim for proportional control.

Functional Electrical Stimulation

Our focus here was to provide a solution for individuals with SCI that would allow them to regain control of their limb movement and avoid overstimulating and fatiguing their affected muscles. As the most stable form of control was achieved for full dorsi-/plantarflexion (Fig. 3E, Fig. 7E, Table 2), we decided that these motor dimensions would be the most appropriate to test. Furthermore, to avoid overstimulating and consequently fatiguing the muscles, we used the stimulation and waiting time parameters integrated within MyoGestic (Fig. 7B) to continuously alternate between stimulating and not stimulating the affected leg.

We showed how two participants could use their spared EMG to trigger an electrical stimulator, significantly increasing their dorsiflexion RoM compared to their pathological RoM ($p < 0.01$, Fig. 7C). This increase in RoM brought their foot movement closer to the typical RoM (here set as 20 degrees for dorsiflexion and 8 degrees for plantarflexion) seen in healthy populations [36] by 33.6% of the typical range for S1 and 40% for S2 during dorsiflexion and by 13.25% for S1 during plantarflexion. In the case of S1, the increase in dorsiflexion RoM starts from an existing, albeit small pathological RoM of 2.79 degrees, while for S2, it begins from almost no movement at -0.31 degrees. For plantarflexion in S1, the use of FES is, however, far less impactful compared to when S1 performed dorsiflexion, since the foot RoM for plantarflexion without FES is already very close to that of the unaffected foot (0.24 degree difference between the RoM of both feet). This may be explained by S1's near-normal RoM during plantarflexion—7.84 degrees without stimulation, reaching 98% of the healthy RoM. However, the muscle grade on the affected side (grade 3) indicates the ability to move against gravity but not against resistance [25]. Future work could explore the potential benefits of our FES system in improving the force output and muscle strength over a longer duration of time.

Interestingly, the difference in dorsiflexion RoM achieved between the affected and unaffected sides while stimulating was much smaller (from 4.12 to 0.81 degrees for S1 and from 18.78 to 1.02 degrees for S2). Furthermore, the correlation coefficient between the affected and unaffected foot movement has also increased to a significant value while using electrical stimulation (0.87 for S1 and 0.6 for S2 during dorsiflexion and 0.96 for S1 during plantarflexion; $p < 0.001$ for all cases). These results indicate that FES has not only helped increase the user RoM closer to the healthy RoM reported in the literature [36], [46], [47], but has also led to a better coordination between the two lower limbs. This highlights the potential of closed-loop FES for improving the neural control in individuals with SCI, as well as its role as an assistive tool in motor recovery.

One limitation of this study which should be highlighted is that the stimulator control was not evaluated in a gait setting. This is, in part, due to the bulky nature of the device (~ 2.1 kg; see Materials and Methods) and the added complexity of integrating it into a gait experiment setting. Future work should explore interfacing our cursor neural interface with a portable stimulator device to enable a closed-loop control in walking activities as well.

MATERIALS AND METHODS

Study design

We recruited five individuals with SCI (denoted as S1-5; Table 1), which consisted of 2 male and 3 female participants with an age mean of 58.8 ± 8.4 years. Five additional healthy participants consisting of 1 female and 4 males with the ages 24.8 ± 2.79 years were recruited for preliminary EMG recordings of maximum voluntary contractions. The data recorded from them and from S1 in offline for model testing was used to optimize the hyperparameters of the CatBoost model before testing it in online with the participants with SCI. Participants provided their written informed consent to participate in the study, which was conducted in accordance with the Declaration of Helsinki. All procedures and experiments were approved by the ethics committees of the Friedrich-Alexander-Universität Erlangen-Nürnberg (applications 24-208-B and 24-286-B approved on the 26th of June 2024 and the 15th of August 2024 respectively). Before the experiments, the participants were given a detailed explanation of the study again and were asked to reaffirm their consent to participate.

For the spinal cord injured participants, the EMG was recorded from one of the motor-affected sides for S1-S4 (Table 1) and from the only motor-affected side for S5 (Table 1). For the healthy participants recruited for the model optimization, the leg that the participants reported as dominant was recorded (left leg for participant 4 and right leg for the rest).

Except for S1, all other participants required walking aids in their daily living at the time of the recording, making gait recording difficult and potentially exhausting for them. For this reason and due to the recent nature of the injury for S3-5 (Table 1), we designed our experiments to focus on one ankle movement at a time. Each experiment was conducted in a single session per participant. Subjects were first introduced to the 2D virtual cursor interface (Fig. 1B, Fig. 2B) and given approximately 5 minutes to try each of the four ankle movements while following the cursor on the screen. For the electrical stimulation experiment, additional time was required to place the reflective camera markers on both legs (~10 minutes). Finally, around 30 minutes were required to identify the suitable stimulation parameters for the participant, specifically the stimulation current and the MyoGestic stimulation control parameters (see Functional Electrical Stimulation), while ensuring they experienced no discomfort.

The EMG bracelet used was placed 12-14 cm below the knee over the bellies of the calf muscles (Fig. 2C). This area was chosen because it contains important muscles relevant to ankle movements, such as the tibialis anterior, gastrocnemius and peroneus longus. In addition, this location reflected the placement of other FES based neuroprostheses [5], [13], [14], which allowed us to evaluate whether the same location could be used for an EMG reading system. Two bracelet lengths were available (23 and 33 cm) and the one closest to the participants leg circumference was selected to ensure good electrode-skin contact and minimal motion artefacts. An adhesive reference electrode (Adhesive electrode 4x4 cm, Axion GmbH, Leonberg, Germany) was attached to the medial malleolus of the leg (Fig. 2D).

The 2D cursor interface used to assess the spared ankle motor dimensions of the participants with SCI and to trigger the electrical stimulation was integrated with our previously published software, MyoGestic [20]. This software was chosen for its flexibility in integrating new output interfaces for individuals with neural lesions into an existing EMG processing pipeline and for enabling easy evaluation of different ML models for myocontrol.

EMG acquisition

The EMG bracelet (HD20MM1602B, OT Bioelettronica S.r.l., Turin, Italy) consisted of 32 dry gold-plated copper electrodes distributed across 2 columns with 16 rows. The inter-electrode distance for the columns was set at 2 cm, while for the rows it varied between 2.1 and 2.2 cm depending on the bracelet length (31.8 and 33 cm respectively) selected and the calf circumference due to the stretchable printed circuit board. A wireless probe (Muovi, OT Bioelettronica S.r.l., Turin, Italy) was used to collect the EMG signals and stream them wirelessly to a host device using a Transmission Control Protocol (TCP) connection. These signals were digitized at 16 bits and sampled at ~ 2000 Hz. The decision to use wireless EMG probes for most of the experiments was motivated both by the desire to minimize motion artifacts caused by cabled connections during leg movements as well as to test an EMG system that could be easily integrated into a wearable orthosis setup in the future. All EMG signals were recorded in monopolar derivation.

Virtual interface

The interface displayed a red cursor that acted both as a visual movement guide for the participant and as a source of ground truth data. The cursor could move either along the X or Y-axis in either direction, depending on the assigned target movements: *up* (dorsiflexion), *down* (plantarflexion), *right* (inversion), *left* (eversion) and *no movement* (rest). The cursor could follow a linear oscillating pattern with adjustable parameters in the user interface, including sampling rate (default: 60 Hz), motion frequency, and holding times at the axis midpoint (rest), endpoints (full contraction), and half-endpoints (partial contraction). During the offline recording for model training and online recording for validating model performance, the reference cursor position was sampled and streamed at 60 Hz using a User Datagram Protocol (UDP) connection.

The Muovi wireless amplifier can stream EMG signals in non-overlapping data windows of 18 samples (~ 9 ms) at a rate of 111 Hz. Since this would not provide sufficient temporal information for a stable ML model prediction, we created a real-time queue that concatenated the latest received EMG windows in a buffer. The buffer length for the single Muovi probe data was set to 504 samples respectively (~ 252 ms).

Each EMG signal was bandpass filtered between 10 and 500 Hz to preserve the relevant MU information associated with surface EMG [17] and notch filtered at 50 Hz to remove the power line interference, both using Butterworth filters. From the filtered signals, one RMS value was computed per channel and stored along with the corresponding movement task label. The first and last 40% of the data was used for model training, while the middle 20% was reserved for testing. Mean and standard deviation were calculated from the training data and used to normalize both the test set as well as all incoming EMG data used for the real-time prediction.

For real-time prediction, a second blue cursor provided feedback to the user based on the ML model output. In the case of a classifier, the cursor position was computed using an exponential decay factor, preset in the user interface (with a default value of 50 used in the experiments for a prediction refresh rate of 111 Hz). Because mapping each classifier label directly to the endpoint of one of the axes displayed on the screen (dorsi-/plantarflexion – upper/lower end of the Y-axis; inversion/eversion – right/left end of the X-axis) would cause abrupt transitions in the cursor position, this decay factor was used to smoothen those transitions. Specifically, it divides the position change over one time step with the decay factor, resulting in smaller step sizes and less jittery movement as the factor is increased.

Models

Two ML algorithms were used throughout this study: a Linear Discriminant Analysis implemented in the scikit-learn library in Python [26] and a Gradient Boosting Decision Tree using the CatBoost implementation [27]. After applying hyperparameter optimization via the Optuna optimization software [31] and using the offline test data recorded from the healthy participants and from S1, the following parameters were identified as optimal for our task: 300 tree iterations with a tree depth of 10 nodes, a learning rate of 0.04 and a L2 regularization factor of 0.014. To speed up the training process, the CatBoost model was trained individually for each participant on an NVIDIA RTX 3070 laptop GPU.

Motion capture setup

Ten infrared tracking cameras (PrimeX 22, OptiTrack, NaturalPoint, Inc., Corvallis, Oregon, USA) were used to record the positions of reflective markers (14 mm, x-base) attached to the measured lower limb using Velcro-friendly shoe wraps for the foot and skin-adhesive tape for the shin. The system, with a tracking error of 0.23 mm achieved after calibration, was suitable for detecting small changes in foot orientation, allowing for detecting subtle changes in the foot movement.

The Motive 3.0.3 software (OptiTrack, NaturalPoint, Inc., Corvallis, Oregon, USA) was used to enable recordings and store motion data, which were recorded at a sampling rate of 120 Hz and then low pass filtered at 2 Hz. Missing values from the recordings due to occlusion were obtained either by linear interpolation or estimated from the neighboring tracked markers. To synchronize the EMG signals and camera data, a graphical user interface automation module in Python was used to control the on-screen position of the mouse cursor to start both recordings [48].

To track the foot, five camera markers were placed on anatomical landmarks of the foot [46] and one marker was placed on the tibia. These six camera markers proved sufficient for our application to calculate the dorsi-/plantarflexion angles. We placed up to six additional markers on both the tibia and foot to help reconstruct the position of key camera markers during camera frames where markers were occluded. Further details of the marker placement and calculation of the ankle angle are shown in Fig. 2C.

Electrical stimulation setup

For the FES, a biphasic constant current stimulator (DS8R, Digitimer Ltd, Welwyn Garden City, United Kingdom) was used to deliver electrical stimulation to the calf muscles of the limb where the EMG signals were measured. This device is suitable for benchtop use (~2.1 kg, 270 x 110 x 225 mm) and allows adjustment of the current in 0.1 mA steps and pulse duration in 10 μ s steps, enabling precise tuning of pulse parameters to meet experimental needs. Furthermore, the device has a built-in pulse energy limit (300 mJ per pulse), ensuring participant safety during prolonged electrical stimulation sessions. The cathode and anode of the stimulator were connected to a pair of adhesive hydrogel cloth electrodes (ValuTrode Cloth Electrodes, Axelgaard Manufacturing Co. Ltd., Fallbrook, California, USA), which were positioned above and below the 32-channel EMG bracelet (Fig. 1D, Fig. 7A). Stimulation electrodes included 4×6 cm oval electrodes and 5×5 square electrodes, placed on the anterior side over the tibialis anterior to elicit dorsiflexion, and on the posterior side over the gastrocnemius medialis to elicit plantarflexion, respectively. The electrodes were placed above and below the EMG bracelet (Fig. 7A).

The stimulation pulse parameters were configured using the front panel of the stimulator, while the pulse train parameters were configured in a newly created MyoGestic tab (Fig. 7B, see Functional Electrical Stimulation). The pulse width duration was set to 300 μ s to minimize muscle fatigue and reduce muscle spasms due to spasticity [49], [50], while the biphasic symmetrical pulse shape was used to prevent damage to the stimulated tissue [51]. The stimulation current, adjustable in 0.1 mA increments, was set individually for each participant at a level at which the stimulation-induced motor contraction would result in a visible movement without causing any pain or discomfort (Table 3). The values for both participants were within the typical range used for transcutaneous electrical stimulation [51] as well as the range observed in other studies on spinal cord injury [52], [53].

Stimulation was triggered by a square wave signal provided by a commercially available development board (Raspberry Pi 4 B, Raspberry Pi Foundation, Cambridge, United Kingdom). A second TCP connection was established between the host device and the development board to transmit both the stimulation pulse train parameters and the current predicted cursor position (Fig. 1D). A pulse duration of 5 μ s and an initial pulse frequency of 35 Hz was used for the trigger signal, which is within the recommended range for eliciting tetanic muscle contractions [51]. In the event of delays experienced in data transmission from the host device to the Pi board, the frequency would be reduced appropriately for each participant.

EMG decomposition

The monopolar surface EMG signals from the bracelet were initially bandpass filtered between 20 and 500 Hz using a second-order Butterworth filter. To identify individual motor units, a blind source separation method known as the convolution kernel compensation algorithm was used to decompose the signals into individual motor units. This analysis was performed using the DEMUSE software (version 4.5; University of Maribor, Slovenia) for automatic detection of discharge times of the motor units. The identified motor unit spike trains were subsequently inspected visually to correct any false positive or false negative detections. From those, only motor units with a pulse-to-noise ratio greater than 26 dB prior to manual inspection were retained.

Statistical Analysis

For the results of the task separation test (see Motor Dimension Separation), A Kruskal-Wallis test ($\alpha=0.05$, one-way, unpaired) was computed over the normalized mean absolute error (nMAE) values across all tasks (Fig. 3E) to assess if there was any statistical difference between the performance achieved for each task. In addition, a Mann-Whitney U test ($\alpha=0.05$, unpaired, two-sided) was used to compare the nMAE values achieved by the LDA and CatBoost models (Fig. 3D). Meanwhile, for the results of the partial EMG activation test (see Proportional Activation), a Kruskal-Wallis test ($\alpha=0.05$) followed by post-hoc two-sided Mann-Whitney U tests were computed over all task groups with Bonferroni correction (Fig. 6E). Both tests are unparametric and were chosen because each task data group had fewer than 10 data points and each model data group had fewer than 30 data points overall. The amount of data was therefore considered insufficient to assume normality for a parametric test.

Furthermore, for the electrical stimulation test (see Functional Electrical Stimulation), a one-way ANOVA test ($\alpha=0.05$) was used to compare RoM achieved for the four task groups (full contraction before/during stimulation and rest before/during stimulation). Following this, post-hoc independent Welch t-tests with Bonferroni correction were used to compare the individual groups (Fig. 7C). Finally, the Pearson correlation coefficient was computed to assess the correlation

between the task accuracy and Jensen-Shannon divergence during partial dorsi-/plantarflexion ($\alpha=0.05$, Fig. 6D), as well as the correlation between the ankle RoM of both feet before and during electrical stimulation ($\alpha=0.05$, Fig. 7D).

ACKNOWLEDGMENTS

We would like to acknowledge Prof. Dr. Dario Farina for reviewing an earlier version of our manuscript.

Competing interests: Authors declare that they have no competing interests.

Data and materials availability: See code for MyoGestic version 0.6.0 at <https://doi.org/10.5281/zenodo.15700021>. All data needed to evaluate the conclusions in the paper are present in the paper.

REFERENCES

- [1] A. Van Der Salm, A. V. Nene, D. J. Maxwell, P. H. Veltink, H. J. Hermens, and M. J. IJzerman, "Gait Impairments in a Group of Patients With Incomplete Spinal Cord Injury and Their Relevance Regarding Therapeutic Approaches Using Functional Electrical Stimulation," *Artificial Organs*, vol. 29, no. 1, pp. 8–14, Jan. 2005, doi: 10.1111/j.1525-1594.2004.29004.x.
- [2] E. Jakubowitz, D. Yao, H. Windhagen, C. Stukenborg-Colsman, A. Thomann, and K. Daniilidis, "Behandlungsoptionen beim neurogenen Lähmungsfuß – eine systematische Literaturrecherche," *Z Orthop Unfall*, vol. 155, no. 04, pp. 402–408, Aug. 2017, doi: 10.1055/s-0043-100760.
- [3] I. Aprile *et al.*, "Multicenter study of peroneal mononeuropathy: clinical, neurophysiologic, and quality of life assessment," *J Peripheral Nervous Sys*, vol. 10, no. 3, pp. 259–268, Sep. 2005, doi: 10.1111/j.1085-9489.2005.10304.x.
- [4] A. Gupta, N. Vardalakis, and F. B. Wagner, "Neuroprosthetics: from sensorimotor to cognitive disorders," *Commun Biol*, vol. 6, no. 1, p. 14, Jan. 2023, doi: 10.1038/s42003-022-04390-w.
- [5] J. M. Hausdorff and H. Ring, "Effects of a New Radio Frequency–Controlled Neuroprosthesis on Gait Symmetry and Rhythmicity in Patients with Chronic Hemiparesis," *American Journal of Physical Medicine & Rehabilitation*, vol. 87, no. 1, pp. 4–13, Jan. 2008, doi: 10.1097/PHM.0b013e31815e6680.
- [6] S. Scott, M. Linden, J. Hooper, P. Cowan, and T. Mercer, "Quantification of gait kinematics and walking ability of people with multiple sclerosis who are new users of functional electrical stimulation," *J Rehabil Med*, vol. 45, no. 4, pp. 364–369, 2013, doi: 10.2340/16501977-1109.
- [7] F. Berenpas, S. Schiemanck, A. Beelen, F. Nollet, V. Weerdesteyn, and A. Geurts, "Kinematic and kinetic benefits of implantable peroneal nerve stimulation in people with post-stroke drop foot using an ankle-foot orthosis," *Restorative Neurology and Neuroscience*, vol. 36, no. 4, pp. 547–558, Jul. 2018, doi: 10.3233/RNN-180822.
- [8] J. Malešević *et al.*, "A decision support system for electrode shaping in multi-pad FES foot drop correction," *J NeuroEngineering Rehabil*, vol. 14, no. 1, p. 66, Dec. 2017, doi: 10.1186/s12984-017-0275-5.
- [9] B. W. Heller *et al.*, "Automated setup of functional electrical stimulation for drop foot using a novel 64 channel prototype stimulator and electrode array: Results from a gait-lab based study," *Medical Engineering & Physics*, vol. 35, no. 1, pp. 74–81, Jan. 2013, doi: 10.1016/j.medengphy.2012.03.012.
- [10] S. Ismail, M. N. Harun, and A. H. Omar, "Functional Electrical Stimulation for Foot Drop Injury Based on the Arm Swing Motion," *Procedia Manufacturing*, vol. 2, pp. 490–494, 2015, doi: 10.1016/j.promfg.2015.07.084.
- [11] L. Meng, B. Porr, C. A. Macleod, and H. Gollee, "A functional electrical stimulation system for human walking inspired by reflexive control principles," *Proc Inst Mech Eng H*, vol. 231, no. 4, pp. 315–325, Apr. 2017, doi: 10.1177/0954411917693879.
- [12] G. P. Braz, M. F. Russold, C. Fornusek, N. A. Hamzaid, R. M. Smith, and G. M. Davis, "A novel motion sensor-driven control system for FES-assisted walking after spinal cord injury: A pilot study," *Medical Engineering & Physics*, vol. 38, no. 11, pp. 1223–1231, Nov. 2016, doi: 10.1016/j.medengphy.2016.06.007.
- [13] S. Xu *et al.*, "Closed-Loop Wearable Device Network of Intrinsically-Controlled, Bilateral Coordinated Functional Electrical Stimulation for Stroke," *Advanced Science*, vol. 11, no. 17, p. 2304763, May 2024, doi: 10.1002/advs.202304763.
- [14] S. Jung, J. H. Bong, K. Kim, and S. Park, "Machine-learning-based coordination of powered ankle-foot orthosis and functional electrical stimulation for gait control," *Front. Bioeng. Biotechnol.*, vol. 11, p. 1272693, Jan. 2024, doi: 10.3389/fbioe.2023.1272693.
- [15] F. Ferrari, E. Zimei, M. Gandolla, A. Pedrocchi, and E. Ambrosini, "An EMG-triggered cooperative controller for a hybrid FES-robotic system," in *2023 IEEE International Conference on Metrology for eXtended Reality, Artificial Intelligence and Neural Engineering (MetroXRINE)*, Milano, Italy: IEEE, Oct. 2023, pp. 852–857. doi: 10.1109/MetroXRINE58569.2023.10405687.

- [16] I. L. Petersen, W. Nowakowska, C. Ulrich, and L. N. S. A. Struijk, "A Novel sEMG Triggered FES-Hybrid Robotic Lower Limb Rehabilitation System for Stroke Patients," *IEEE Trans. Med. Robot. Bionics*, vol. 2, no. 4, pp. 631–638, Nov. 2020, doi: 10.1109/TMRB.2020.3019081.
- [17] R. Merletti and P. Parker, Eds., *Electromyography: Physiology, Engineering, and Noninvasive Applications*, 1st ed. Wiley, 2004. doi: 10.1002/0471678384.
- [18] A. L. Cakici *et al.*, "A Generalized Framework for the Study of Spinal Motor Neurons Controlling the Human Hand During Dynamic Movements," in *2022 44th Annual International Conference of the IEEE Engineering in Medicine & Biology Society (EMBC)*, Glasgow, Scotland, United Kingdom: IEEE, Jul. 2022, pp. 4115–4118. doi: 10.1109/EMBC48229.2022.9870914.
- [19] D. S. Oliveira *et al.*, "A direct spinal cord–computer interface enables the control of the paralysed hand in spinal cord injury," *Brain*, vol. 147, no. 10, pp. 3583–3595, Oct. 2024, doi: 10.1093/brain/awae088.
- [20] R. C. Sîmpetru *et al.*, "MyoGestic: EMG interfacing framework for decoding multiple spared motor dimensions in individuals with neural lesions," *Sci. Adv.*, vol. 11, no. 15, p. eads9150, Apr. 2025, doi: 10.1126/sciadv.ads9150.
- [21] J. M. Hahne, M. A. Schweisfurth, M. Koppe, and D. Farina, "Simultaneous control of multiple functions of bionic hand prostheses: Performance and robustness in end users," *Sci. Robot.*, vol. 3, no. 19, p. eaat3630, Jun. 2018, doi: 10.1126/scirobotics.aat3630.
- [22] E. N. Kamavuako, M. Brown, X. Bao, I. Chihi, S. Pitou, and M. Howard, "Affordable Embroidered EMG Electrodes for Myoelectric Control of Prostheses: A Pilot Study," *Sensors*, vol. 21, no. 15, p. 5245, Aug. 2021, doi: 10.3390/s21155245.
- [23] M. Nowak, I. Vujaklija, A. Sturma, C. Castellini, and D. Farina, "Simultaneous and Proportional Real-Time Myocontrol of Up to Three Degrees of Freedom of the Wrist and Hand," *IEEE Trans. Biomed. Eng.*, vol. 70, no. 2, pp. 459–469, Feb. 2023, doi: 10.1109/TBME.2022.3194104.
- [24] R. Rupp *et al.*, "International Standards for Neurological Classification of Spinal Cord Injury," *Topics in Spinal Cord Injury Rehabilitation*, vol. 27, no. 2, pp. 1–22, Mar. 2021, doi: 10.46292/sci2702-1.
- [25] U. Naqvi and A. L. Sherman, "Muscle Strength Grading," in *StatPearls*, Treasure Island (FL): StatPearls Publishing, 2025. Accessed: Apr. 24, 2025. [Online]. Available: <http://www.ncbi.nlm.nih.gov/books/NBK436008/>
- [26] F. Pedregosa *et al.*, "Scikit-learn: Machine Learning in Python," *MACHINE LEARNING IN PYTHON*.
- [27] L. Prokhorenkova, G. Gusev, A. Vorobev, A. V. Dorogush, and A. Gulin, "CatBoost: unbiased boosting with categorical features".
- [28] M. S. AL-Quraishi *et al.*, "Classification of ankle joint movements based on surface electromyography signals for rehabilitation robot applications," *Med Biol Eng Comput*, vol. 55, no. 5, pp. 747–758, May 2017, doi: 10.1007/s11517-016-1551-4.
- [29] A. Noor *et al.*, "Decoding of Ankle Joint Movements in Stroke Patients Using Surface Electromyography," *Sensors*, vol. 21, no. 5, p. 1575, Feb. 2021, doi: 10.3390/s21051575.
- [30] K. R. Lyons and S. S. Joshi, "A case study on classification of foot gestures via surface electromyography," presented at the Proc. Annu. Conf. Rehabil. Eng. Assist. Technol. Soc. Amer, 2015, pp. 1–5.
- [31] T. Akiba, S. Sano, T. Yanase, T. Ohta, and M. Koyama, "Optuna: A Next-generation Hyperparameter Optimization Framework," in *Proceedings of the 25th ACM SIGKDD International Conference on Knowledge Discovery & Data Mining*, Anchorage AK USA: ACM, Jul. 2019, pp. 2623–2631. doi: 10.1145/3292500.3330701.
- [32] C. Goodall, "Procrustes Methods in the Statistical Analysis of Shape," *Journal of the Royal Statistical Society Series B: Statistical Methodology*, vol. 53, no. 2, pp. 285–321, Jan. 1991, doi: 10.1111/j.2517-6161.1991.tb01825.x.
- [33] F. Negro, A. Holobar, and D. Farina, "Fluctuations in isometric muscle force can be described by one linear projection of low-frequency components of motor unit discharge rates," *The Journal of Physiology*, vol. 587, no. 24, pp. 5925–5938, Dec. 2009, doi: 10.1113/jphysiol.2009.178509.
- [34] J. Lin, "Divergence measures based on the Shannon entropy," *IEEE Trans. Inform. Theory*, vol. 37, no. 1, pp. 145–151, Jan. 1991, doi: 10.1109/18.61115.
- [35] F. Biering-Sørensen, J. B. Nielsen, and K. Klinge, "Spasticity-assessment: a review," *Spinal Cord*, vol. 44, no. 12, pp. 708–722, Dec. 2006, doi: 10.1038/sj.sc.3101928.
- [36] A. Silder, B. Heiderscheit, and D. G. Thelen, "Active and passive contributions to joint kinetics during walking in older adults," *Journal of Biomechanics*, vol. 41, no. 7, pp. 1520–1527, Jan. 2008, doi: 10.1016/j.jbiomech.2008.02.016.
- [37] S.-H. Liu, A. K. Sharma, B.-Y. Wu, X. Zhu, C.-J. Chang, and J.-J. Wang, "Estimating gait parameters from sEMG signals using machine learning techniques under different power capacity of muscle," *Sci Rep*, vol. 15, no. 1, p. 12575, Apr. 2025, doi: 10.1038/s41598-025-95973-0.
- [38] R. Q. Y. Chia, "Classification of Spinal Cord Injured EMG Data for Locomotion Recovery," University of Technology Sydney (Australia), 2024.
- [39] D. S. D. Oliveira, M. Carbonaro, B. J. Raiteri, A. Botter, M. Ponfick, and A. Del Vecchio, "The discharge characteristics of motor units innervating functionally paralyzed muscles," *Journal of Neurophysiology*, vol. 133, no. 2, pp. 343–357, Feb. 2025, doi: 10.1152/jn.00389.2024.
- [40] M. Oßwald, A. L. Cakici, D. Souza De Oliveira, D. I. Braun, D. Farina, and A. Del Vecchio, "Task-specific motor units in the extrinsic hand muscles control single- and multidigit tasks of the human hand," *Journal of Applied Physiology*, vol. 138, no. 5, pp. 1187–1200, May 2025, doi: 10.1152/jappphysiol.00911.2024.
- [41] R. Wang and E. M. Gutierrez-Farewik, "The effect of subtalar inversion/eversion on the dynamic function of the tibialis anterior, soleus, and gastrocnemius during the stance phase of gait," *Gait & Posture*, vol. 34, no. 1, pp. 29–35, May 2011, doi: 10.1016/j.gaitpost.2011.03.003.

- [42] A. M. Van Leeuwen, J. H. Van Dieën, A. Daffertshofer, and S. M. Bruijn, "Ankle muscles drive mediolateral center of pressure control to ensure stable steady state gait," *Sci Rep*, vol. 11, no. 1, p. 21481, Nov. 2021, doi: 10.1038/s41598-021-00463-8.
- [43] S. Kirshblum, B. Snider, F. Eren, and J. Guest, "Characterizing Natural Recovery after Traumatic Spinal Cord Injury," *Journal of Neurotrauma*, vol. 38, no. 9, pp. 1267–1284, May 2021, doi: 10.1089/neu.2020.7473.
- [44] C. M. Gregory *et al.*, "Resistance training and locomotor recovery after incomplete spinal cord injury: a case series," *Spinal Cord*, vol. 45, no. 7, pp. 522–530, Jul. 2007, doi: 10.1038/sj.sc.3102002.
- [45] R. C. Simpetru, D. Souza De Oliveira, M. Ponfick, and A. Del Vecchio, "Identification of Spared and Proportionally Controllable Hand Motor Dimensions in Motor Complete Spinal Cord Injuries Using Latent Manifold Analysis," *IEEE Trans. Neural Syst. Rehabil. Eng.*, vol. 32, pp. 3741–3750, 2024, doi: 10.1109/TNSRE.2024.3472063.
- [46] A. Leardini, M. G. Benedetti, L. Berti, D. Bettinelli, R. Nativo, and S. Giannini, "Rear-foot, mid-foot and fore-foot motion during the stance phase of gait," *Gait & Posture*, vol. 25, no. 3, pp. 453–462, Mar. 2007, doi: 10.1016/j.gaitpost.2006.05.017.
- [47] B. Baggett and G. Young, "Ankle joint dorsiflexion. Establishment of a normal range," *J Am Podiatr Med Assoc*, vol. 83, no. 5, pp. 251–254, May 1993, doi: 10.7547/87507315-83-5-251.
- [48] A. Sweigart, *asweigart/pyautogui*. (Jan. 14, 2025). Python. Accessed: Jan. 14, 2025. [Online]. Available: <https://github.com/asweigart/pyautogui>
- [49] A. H. Bekhet, V. Bochezanian, I. M. Saab, and A. S. Gorgey, "The Effects of Electrical Stimulation Parameters in Managing Spasticity After Spinal Cord Injury: A Systematic Review," *Am J Phys Med Rehabil*, vol. 98, no. 6, pp. 484–499, Jun. 2019, doi: 10.1097/PHM.0000000000001064.
- [50] T. Kesar and S. Binder-Macleod, "Effect of frequency and pulse duration on human muscle fatigue during repetitive electrical stimulation," *Experimental Physiology*, vol. 91, no. 6, pp. 967–976, Nov. 2006, doi: 10.1113/expphysiol.2006.033886.
- [51] C. Marquez-Chin and M. R. Popovic, "Functional electrical stimulation therapy for restoration of motor function after spinal cord injury and stroke: a review," *BioMed Eng OnLine*, vol. 19, no. 1, p. 34, Dec. 2020, doi: 10.1186/s12938-020-00773-4.
- [52] N. Sanna *et al.*, "Evaluating the health and fitness benefits of a 6-month FES-cycling program on a recumbent trike for individuals with motor complete SCI: a pilot study," *J NeuroEngineering Rehabil*, vol. 22, no. 1, p. 55, Mar. 2025, doi: 10.1186/s12984-025-01585-0.
- [53] D. R. Dolbow, A. S. Gorgey, D. R. Gater, and J. R. Moore, "Body composition changes after 12 months of FES cycling: case report of a 60-year-old female with paraplegia," *Spinal Cord*, vol. 52, no. S1, pp. S3–S4, Jun. 2014, doi: 10.1038/sc.2014.40.